Journal of Remote Sensing
A SCIENCE PARTNER JOURNAL

RESEARCH ARTICLE

Potential of NASA's Plankton, Aerosol, Cloud, and Ocean Ecosystem (PACE) Satellite Observations in the Oxygen Bands for Determining Aerosol Layer Height over Ocean

Xiaoguang Xu[1*], Xi Chen[2*], Jun Wang[2], and Lorraine A. Remer[1]

[1]Earth and Space Institute, and GESTAR2, University of Maryland, Baltimore County, Baltimore, MD 21250, USA. [2]Center for Global and Regional Environmental Research and Iowa Technology Institute, The University of Iowa, Iowa City, IA 52242, USA.

*Address correspondence to: xxu@umbc.edu (X.X.); xi-chen-4@uiowa.edu (X.C.)

Citation: Xu X, Chen X, Wang J, Remer LA. Potential of NASA's Plankton, Aerosol, Cloud, and Ocean Ecosystem (PACE) Satellite Observations in the Oxygen Bands for Determining Aerosol Layer Height over Ocean. *J. Remote Sens.* 2024;4:Article 0167. https://doi.org/10.34133/remotesensing.0167

Submitted 5 February 2024
Accepted 29 May 2024
Published 23 July 2024

Aerosol layer height (ALH) is an important but uncertain parameter for evaluating the impact of aerosols on weather and climate and for accurate atmospheric correction. This study aims to assess the potential for measuring ALH by the Ocean Color Instrument (OCI) on NASA's Plankton, Aerosol, Cloud, ocean Ecosystem satellite. OCI measures Earth-reflected solar spectrum including reflectance in the oxygen (O_2) A and B absorption bands that are invaluable for determining ALH. We assessed the sensitivity and information contained therein in retrieving ALH over the ocean surface by using the radiative transfer simulation of OCI observations in the O_2 bands. The capabilities were also demonstrated using hyperspectral data measured by the TROPOspheric Monitoring Instrument (TROPOMI), as spectrally convolved into the OCI bands. Our results indicate that (a) OCI observations in the O_2 A band are sensitive to ALH, whereas those around the O_2 B band have relatively reduced sensitivity; (b) the most pronounced sensitivity to ALH is found in the 762.5 nm (and 690 nm) around the oxygen A (and B) bands, which are selected for ALH retrievals in this study; and (c) the ALH retrieved from OCI proxy data is in good agreement with the aerosol profile probed by CALIOP lidar. Overall, the ALH retrievals for both smoke and dust events exhibit a root mean square error of 0.49 km and 0.31 km, respectively, for the smoke and dust cases, aligning with the uncertainties of ALH as measured from the concurrent TROPOMI and the Earth Polychromatic Imaging Camera instruments. Therefore, this study suggests from OCI observations that we can generate ALH products with a well-characterized uncertainty. The technique and results presented in this study are suitable to develop a simple but robust ALH algorithm for OCI observations when the data become available.

Introduction

Launched in early 2024, NASA's Plankton, Aerosol, Cloud, and ocean Ecosystem (PACE) mission aims to extend and improve key systemic ocean color, aerosol, and cloud data records for Earth system and climate studies [1,2]. PACE satellite carries an advanced spectrometer, the Ocean Color Instrument (OCI), as its primary payload to measure Earth-reflected solar radiation from ultraviolet (UV) to shortwave-infrared (SWIR) spectrum, providing detailed information on global ocean biology. The spacecraft is also crewed by 2 polarimeters, the Hyper-Angular Rainbow Polarimeter 2 (HARP2) and the Spectro-polarimeter for Planetary Exploration (SPEXone), to measure both intensity and polarization of light from multi-view directions and thus provide critical aerosol measurements for improved OCI ocean remote sensing. Together, PACE observations will extend and improve NASA's decades of data records of ocean color, aerosol, and clouds, providing valuable information for Earth system and climate studies.

Atmospheric aerosols over ocean surface represent a major impediment for accurate remote sensing of ocean color. Their scattering and absorption of solar radiation contributed to the reflected light as observed by satellite sensors. The retrieval of water leaving radiance from ocean surface thus requires taking away the contribution from aerosols and atmosphere, a process known as atmospheric correction [3]. A good atmospheric correction relies on accurate characterization of aerosol optical properties as well as aerosol vertical distribution for absorbing aerosols [4,5]. However, the vertical distribution of aerosols is one of most poorly observed variables from passive aerosol remote sensing techniques [6]. In other words, aerosol height information is needed along with aerosol optical properties for improved OCI atmospheric correction.

In addition to atmospheric correction, aerosol height information is also critical for retrieving aerosol absorption, studying aerosol-cloud interaction, and monitoring surface air quality from satellite data products. For instance, absorbing aerosols such as biomass-burning smoke and mineral dust often enter and reside at a wide range of atmospheric layers depending on the weather conditions. Knowing their vertical location simultaneously is key to accurately determine their amount and

ability of absorbing solar radiation (i.e., aerosol optical depth and single scattering albedo); those aerosol properties are equally important to understand aerosol radiative cooling or heating of the atmosphere and their potential impact in cloud formation and lifetime (e.g., [7]). Those variables are thus equally important for reducing the uncertainty of aerosols' radiative effects to weather and climate. Moreover, the altitude of an aerosol plume characterizes the amount of particulate matters distributed within the lower atmospheric level and regulates how distant the particulate pollution can transport in the downwind direction ([8,9]). Therefore, aerosol layer height (ALH) is a valuable measurement not only for the PACE missions, but also for aerosol study in general.

Inspiringly, PACE instruments are designed to allow aerosol height retrievals from 3 different passive remote sensing perspectives. First, radiance in the oxygen (O_2) A and B absorption bands, such as those observed by both the OCI and SPEXone, is sensitive to the vertical height of scattering aerosols. This is because the presence of an aerosol layer scatters solar light back into space, thus reducing the chance of photons being absorbed by underneath O_2 molecules. The higher the aerosol layer, the less chance for photons being absorbed, leading to enhanced radiance as observed by satellite. Previous studies have also demonstrated that observations in the A and B bands are complementary to each other, considering the spectrally distinct aerosol scattering and surface reflectance [10]. Second, multi-angle polarization data in blue bands, which are available from both HARP2 and SPEXone instruments, are also useful for determining aerosol and cloud heights [11,12]. In contrast to the O_2 band technique, this approach makes use of the intrinsic difference of polarization properties between air molecules (i.e., Rayleigh scattering) and aerosol particles. In particular, the presence of an absorbing aerosol layer shields the strong Rayleigh scattering signals in blue wavelengths, thus reducing polarization signals in the scattering angle range of 80° to 120°, and such reduction is sensitive to aerosol microphysical properties and aerosol vertical height. Third, multi-view imagery by HARP2 and SPEXone will also allow the stereo-height retrievals for texture-rich aerosol plumes using the parallax technique [13,14]. Such technique can provide an efficient and simple height estimate for texture-rich aerosol plumes, such as smoke, volcanic ash, and dust aerosol near source regions. These 3 techniques are not new for PACE observations. Their applications have a long history with dozens of satellite instruments dated back to the 1990s. The physical principles of these retrieval approaches and applications to relevant observations have been reviewed by Xu et al. [6].

In this paper, we focus our study on the first technique that uses OCI O_2 band observations. Meanwhile, it is noted that those 3 techniques have different advantages and would complement each other in retrieval aerosol height; the synergistic study of those techniques is beyond the scope of this paper and will be conducted in a follow-up study. The goal of this study is to provide a pre-launch theoretical analysis as well as retrieval demonstration for determining ALH from PACE OCI observations in both the O_2 A and B bands. To achieve that, we first use radiative transfer modeling to analyze the sensitivity of OCI observations in the O_2 A and B bands to the layer height of aerosols over ocean surface under various aerosol scenarios. We then apply our previously developed ALH retrieval algorithm with OCI proxy observation data from a similar satellite sensor, the TROPOspheric Monitoring Instrument (TROPOMI) [8]. The retrieval accuracy in the ALH from those proxy data is evaluated against space-lidar observations by the Cloud-Aerosol Lidar with Orthogonal Polarization (CALIOP).

This article is organized as follows. The "Materials and Methods" section introduces the detailed methodology on both the theoretical analysis and proxy data retrieval approaches. Results of the sensitivity and error analysis are presented in the "Selected OCI Channels for Aerosol Height Retrieval" section, while retrieval demonstration and validation presented in the "ALH Retrievals Using TROPOMI as an OCI Proxy" section. We summarize the findings and discuss future developments in the "Summary and Implications" section.

Materials and Methods

Theoretical analysis and real-data demonstration are 2 major themes of this study. The theoretical analysis involves sensitivity assessment for synthetic OCI observations in the O_2 A and B bands to the vertical layer height of aerosols. Here, the synthetic OCI data are simulated by the UNified Linearized Vector Radiative Transfer Model (UNL-VRTM) for dust and smoke aerosol types under different surface conditions. The real-data demonstration is accomplished through retrieving ALH from the TROPOMI observations for dust and smoke aerosol cases that are spectrally convolved into OCI spectral bands. In this section, we first describe the OCI and TROPOMI instrumental characteristics, showing the potential of resembling OCI data from observations of the other instrument. Then, we describe the UNL-VRTM model used for OCI band selection analysis and for constructing retrieval lookup tables. Finally, we briefly describe the ALH retrieval algorithm accommodated for OCI instrument.

Proxy OCI data from TROPOMI

As PACE's primary payload, OCI is an advanced spectrometer aimed at daily global remote sensing of ocean biology [15]. It measures Earth-reflected solar radiation from the UV at 340 nm to near-infrared (NIR) at 890 nm at a spectral resolution of about 5 nm and spectral steps of 2.5 nm. The instrument also assembles a radiometer to measure light intensity in 7 discrete bands from 940 nm to 2,260 nm in the SWIR spectrum. The field of view of OCI is ±56.5° across the orbital track, spanning a ground swath width of 2,663 km. Earth view data acquired by OCI have a spatial footprint of 1 km × 1 km.

TROPOMI is a hyperspectral imager onboard the Copernicus Sentinel-5 Precursor satellite launched in October 2017, aimed at measurement of atmospheric trace gases, clouds, and aerosols [16]. It includes 4 separate spectrometers with bands in the UV, visible, NIR, and SWIR spectrum. In its NIR spectral range (i.e., 661 to 786 nm), TROPOMI observes Earth-reflected solar radiance with a spectral resolution of ~0.35 nm and a spectral sampling (~0.126 nm) that are much finer than those of OCI. The instrument operates in a push-broom manner with a swath width of about 2,600 km on the Earth surface at a spatial resolution of 5.5 km along track and 3.5 km cross track. Therefore, its hyperspectral measurements, if convolved into OCI bands, can serve as a good proxy to represent OCI observations with a spatial resolution close to that of the PACE Level 1C data products (i.e., 5.2 km). A briefly side-by-side comparison of OCI and TROPOMI observations is listed in Table.

Figure 1 illustrates OCI's spectral response functions in the context of O_2 absorption spectrum around the O_2 A and B bands.

Table. Comparison of OCI and TROPOMI observations

	OCI	TROPOMI
Spectral coverage in UV to NIR	340–895 nm	267–499 nm; 661–786 nm
SWIR bands	940, 1,038, 1,250, 1,378, 1,615, 2,130, 2,260 nm	2,300–2,389 nm
Spectral step of NIR bands	2.5 nm	0.126 nm
Spectral resolution of NIR bands	5.0 nm	0.34–0.35 nm
Orbit altitude	676.5 km	824 km
Orbit inclination	98	98.7
Local overpass time	~13:00	~13:30
Swath width	2,660 km	2,600 km
Level 1B pixel resolution	1.2 km × 1.2 km at nadir for all bands	5.5 km × 3.5 km for most bands, 5.5 km × 7.0 km for SWIR bands
Level 1C grid size	5.2 km × 5.2 km	N/A

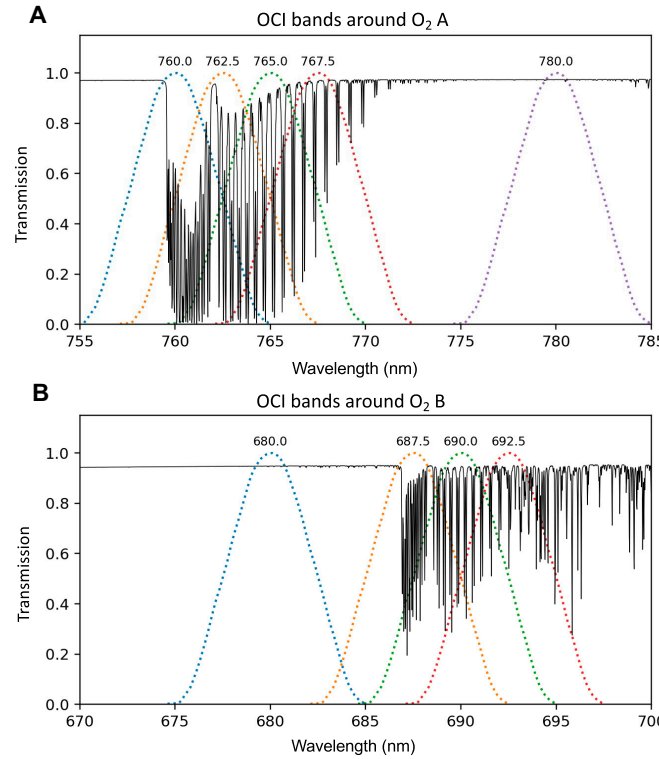

Fig. 1. Atmospheric transmission around O_2 A (A) and B (B) bands overlaid by a simulated OCI reflectance spectral response.

We select 2 OCI outer continuum bands, i.e., at 780 nm and 680 nm, each around the A and B bands, respectively. Several OCI channels within the O_2 absorption spectral region are chosen as candidates; they are 760, 762.5, 765, and 767.5 nm in the O_2 A band and 687.5, 690, and 692.5 in the O_2 B band. We do not intend to use all those bands in the height retrievals; instead, we use the band with the strongest height sensitivity in each of the A and B bands, as identified by a sensitivity analysis.

Several additional channels are also needed for screening cloud, determining aerosol type (i.e., dust and smoke separation), characterizing surface, and constraining aerosol optical depth. Following the ALH retrieval algorithm in Chen et al. [8], a blue channel at 442.5 nm and a SWIR at 2,130 nm will be selected.

Model-based approach for the selection of OCI bands

We utilize radiative transfer simulations of OCI radiance data in the O_2 bands to assess the sensitivity of those measurements to the change of vertical profile of 2 commonly aloft aerosol types: smoke and mineral dust. As indicated by many previous studies [4,17–19], the color ratio of top-of-the-atmosphere (TOA) radiance around the O_2 bands is often used to detect ALH, whereas the TOA radiance in the nearby non-absorbing band is only sensitive to aerosol loading. We focus the sensitivity analysis on the corresponding 2 observed variables: (a) reflectance in an outer band (aka continuum band) of each of the O_2 A and B spectral regions, and (b) the reflectance ratios of inner bands to the continuum band around both O_2 bands. The candidate OCI bands around the O_2 A and B bands are indicated in Fig. 1.

Simulation of OCI radiance uses the UNL-VRTM, which was specifically designed as a testbed for remote sensing of the Earth atmosphere and surface, with special emphasis for aerosols ([20,21]; https://unl-vrtm.org). UNL-VRTM provides a rigorous and complete treatment of required physical processes for simulating remote sensing data, through integration of the VLIDORT radiative transfer model [22,23] with modules dealing with absorption of trace gases, molecular and particle scattering, and surface reflection. It has been used to retrieve aerosol, cloud, nitrogen dioxide, and surface information from a variety of existing and future remote sensing instruments (e.g., [24–27]). Detailed development, validation, and applications of the model were described by Xu and Wang [21].

Specifically for this study, UNL-VRTM simulations are performed at a high spectral resolution of 0.02 nm and then are spectrally convolved to the considered OCI bands shown in Fig. 1. Simulations are performed for dust and smoke aerosols with various AOD values and ALH values, from which we can identify the absorption bands in each of the O_2 A and B spectral regions that are most sensitive to the change of ALH.

Following our previous studies [8,10,19], aerosol vertical profile extends from surface to an altitude of 15 km and is assumed to follow a quasi-Gaussian distribution function,

$$\beta(z) = \frac{W\exp(-c|z-H|)}{\left[1+\exp(-c|z-H|)\right]^2}, \quad (1)$$

where $\beta(z)$ represents aerosol extinction coefficient at height z; as such, the column AOD is calculated by $\mathrm{AOD} = \int_0^{15\ \mathrm{km}} \beta(z)dz$. W is a constant related to AOD, and H is the ALH at which the aerosol extinction has its peak. When $H = 0$, the profile function becomes an exponential decay function. c is related to the half width (η)

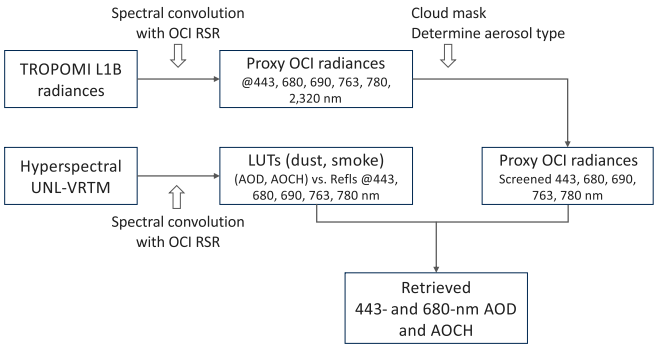

Fig. 2. Flowchart of retrieving AOCH from OCI proxy datasets.

of vertical profile by $c = ln\left(3+\sqrt{8}\right)/\eta$, and $\eta = 1.0$ km is assumed. As such, the ALH represents the aerosol optical centroid height, or AOCH. Thus, the terms of ALH and AOCH are used interchangeably in this study. Aerosol optical models representing dust and smoke are identical to the ones used in Chen et al. [8], which were also used for building lookup tables for retrieving ALH from the Earth Polychromatic Imaging Camera (EPIC) on the Deep Space Climate Observatory (DSCOVR) satellite [10,19].

ALH retrieval algorithm applied to OCI proxy data

In the current study, TROPOMI-observed hyperspectral radiance is used as OCI proxy data to showcase the "O_2" aerosol height retrieval. The retrieval algorithm was initially developed by Xu et al. [10,19] and gained substantial enhancement by Chen et al. [8] for improved cloud screening and aerosol type identification. In this study, the algorithm is applied to 6 selected OCI bands, 442.5, 680, 690, 762.5, 780, and 2,320 nm, the selection of which is presented in the "Selected OCI Channels for Aerosol Height Retrieval" section. It is noted that the TROPOMI SWIR band of 2,230 nm is used for cloud screening and aerosol type classification, but not for determining AOD and AOCH. The corresponding band from OCI is centered at 2,130 nm. The lookup tables that were used by Chen et al. [8] are reconstructed using UNL-VRTM simulations with inputs of the same aerosol models and geometrical tables, but with OCI spectral response functions applied for calculating radiance at each of those selected OCI bands.

A detailed algorithm theory and considerations are described in Chen et al. [8] and Xu et al. [10,19]. Figure 2 presents a flowchart of procedures of retrieving AOD and AOCH from the proxy OCI data, which involve the following steps: (a) Perform spectral convolution on the TROPOMI level-1B radiance into OCI bands and resample the proxy OCI data in all the used bands into the same geolocation grid. This step indeed will be unnecessary for real PACE Level 1C datasets that have all bands collocated onto a common grid. (b) Identify surface locations covered by either water surface or vegetated surface that are suitable for aerosol height retrieval. The vegetated land surface is identified by the normalized differential vegetation index above 0.2. (c) Mask cloud pixels with a variety of brightness and homogeneity tests. (d) Classify aerosol type (i.e., smoke or dust) and associate the location to the corresponding aerosol LUT. (e) Determine the AOD at the 443-nm and 680-nm bands together with the AOCH by fitting the observed radiances in the O2 A and B bands with the LUT. Here, AOCH retrieval is considered valid only when the 680-nm AOD exceeds 0.2.

Results

Selected OCI Channels for Aerosol Height Retrieval

As described in the "Model-based approach for the selection of OCI bands" section, UNL-VRTM simulations are performed to evaluate the sensitivity of OCI-observed radiance in O_2 A and B spectral regions to ALH, from which one can identify the most useful bands to be included in the algorithm for determining ALH. These simulations considered both smoke and dust aerosols with various AOD values from 0 to 3.0 and ALH values from 0.5 to 12.5 km. Figure 3 presents the simulated sensitivity of 2 observed quantities (i.e., reflectance in the continuum band and ratio of reflectance between the absorption band and continuum band) with respect to 2 retrieval quantities (680-nm AOD and ALH) for the considered bands in the O_2 A and B spectral regions. Results for other view geometry and dust aerosols present a similar pattern and are thus not shown here. Notably, the reflectance in the 780-nm continuum band increases with rising AOD values, and this correlation remains largely unaffected by the changes in ALH. The ratio of reflectance between absorption bands and continuum bands exhibits sensitivity to ALH. Such sensitivity is different for different absorptions bands and becomes more pronounced as the AOD value increases.

Among the 4 OCI bands within the O_2 A spectral region, Fig. 3C illustrates that the 762.5-nm band displays the most pronounced variability in response to the changes in ALH, followed by the 760- and 765-nm bands. Comparatively, the 767.5-nm band provides the least informative data. Similarly, among those 3 bands within the O_2 B spectral region, the 687.5- and 690-nm bands demonstrate similar sensitivity to ALH changes, while the 692.5-nm band presents the least sensitivity, as depicted in Fig. 3D. As a result, the spectral wavelengths of 762.5 nm in the A band and 690 nm in the B band are chosen for inclusion in the retrieval algorithm.

However, it is noted that the sensitivity to ALH in the O_2 A band is more pronounced than that in the O_2 B band (Fig. 3B), primarily due to the weaker oxygen absorption in the latter. Notwithstanding the difference, it is useful to include both spectral bands in the ALH retrieval, because surface reflectance tends to be much higher over land in the O_2 A band, which substantially reduces the sensitivity. Previous studies have demonstrated that the combined information from both the O_2 A and B bands would allow ALH retrievals over both land and ocean surfaces [8,10].

ALH Retrievals Using TROPOMI as an OCI Proxy

Two aerosol events captured by the TROPOMI representing different aerosol types are used for testing AOCH retrievals from the OCI proxy data. They were among the studied cases in Chen et al. [8] to demonstrate aerosol height retrievals from the TROPOMI observations in the O_2 bands. Figures 4 and 5 display TROPOMI-observed reflectance spectrally convolved into 6 selected OCI bands for those 2 events, respectively. The first case was for smoke plumes erupted from the Camp fire, which was the deadliest and most destructive wildfire in California. As shown in Fig. 4, TROPOMI observed the smoke scene on 2020 November 10, 3 days after the Camp fire started. An RGB

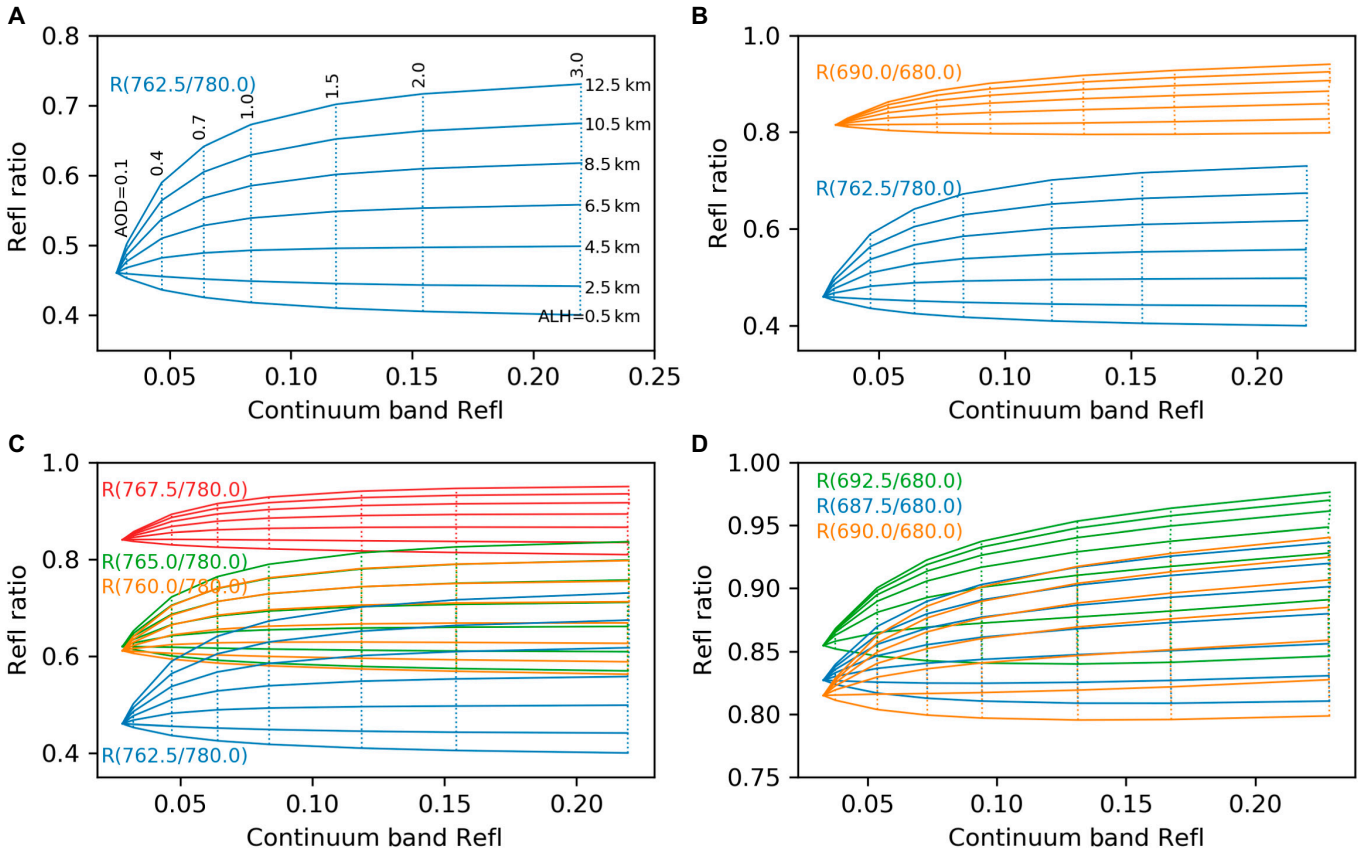

Fig. 3. UNL-VRTM simulated sensitivities of OCI observations around the O_2 A and B bands to various ALH and AOD values (indicated by solid and dotted lines) for biomass-burning smoke. The *x*-axis of these plots represents the continuum band reflectance at 780 nm and 680 nm, whereas the *y*-axis indicates reflectance ratio between the absorption bands to the continuum band in each of the O_2 A and B spectra regions. Four panels show the results for using different OCI spectral pairs: (A) 762.5 nm and 780 nm in the O_2 A shown as blue curves; (B) same as (A) but also adding the 690 nm and 680 nm in the O_2 B region in orange color; (C) for all four, consider OCI bands in the O_2 A; (D) for all three, consider OCI bands in the O_2 B. AOD and ALH values of each grid line are annotated in (A). Spectral wavelengths are annotated as different colors in each panel. Surface albedo of 0.02 is assumed for all bands to approximate an ocean surface, and simulations are performed for a solar zenith angle of 0° and a view zenith angle of 31°.

composite is included in Fig. 6A, showing thick smoke plumes, fanned by strong northeasterly winds, and transported over the west coast of the United States and the Pacific Ocean. The plumes are evident in the OCI's blue, red, and NIR bands, but are optically transparent in the 2,320-nm SWIR band (Fig. 4F). Such spectral variation manifests the sub-micron size of smoke particles, because of which the smoke scattering efficiency substantially decreases as the spectral wavelength increases [28]. Some stripe-shaped gaps are noted on the SWIR band image, which were known TROPOMI measurement artifacts.

The second testing case is for dust aerosols from the Sahara desert transported over the Atlantic on 2019 March 2, as shown in the RGB composite in Fig. 6D. Plots of TROPOMI reflectance spectrally convolved to the OCI bands are presented in Fig. 5, showing bright dust plumes over the dark ocean surface. In contrast to the smoke case, the dust plumes are visible over all the selected OCI channels including the SWIR band. This is because dust particles are much larger in size than smoke aerosols, and so does their scattering efficiency in the SWIR band.

The retrieval algorithm, as accommodated for OCI spectral bands, is applied to the above OCI proxy data for retrieving 680-nm AOD and AOCH. The retrieval results for both aerosol events are shown in Fig. 6. The retrieved 680-nm AOD values, shown in the central panels, are generally over 0.2 for both the smoke and dust plumes, with which threshold the AOCH was retrieved. The stripe gaps on the retrieval reflect the measurement artifact in the SWIR band shown in Fig. 4F. According to Chen et al. [8], a comparison against a limited number of collocated sunphotometer AOD observations at the AERosol RObotic NETwork (AERONET) sites showed that most of the AOD retrievals (~72%) were constrained within the uncertainty of $\pm(0.05 + 10\ \%\ \mathrm{AOD})$. We found no obvious difference of AOD retrievals between this study and Chen et al. [8] for the same aerosol events.

The retrieved AOCH values, shown in the right panels, extended from about 0.5 km to 5 km. In the instance of the Camp fire event, smoke plumes over ocean were predominantly positioned within about 1- to 3-km altitudes in the 32° to 35° latitude regions, whereas the AOCH values were elevated to a range of 3 to 5 km noted in the further south around 30° latitude. In contrast, the AOCH retrievals for the dust aerosols over ocean were around 1 km, indicating a low-level dust layer.

While this study primarily emphasizes the retrieval demonstration over oceanic surfaces, the retrieval algorithm was also applied to terrestrial surfaces. Such retrieval results over land, which were not within the scope of the current study, necessitate further assessment. Nevertheless, an initial qualitative analysis indicates a gradual and consistent transition in the AOD

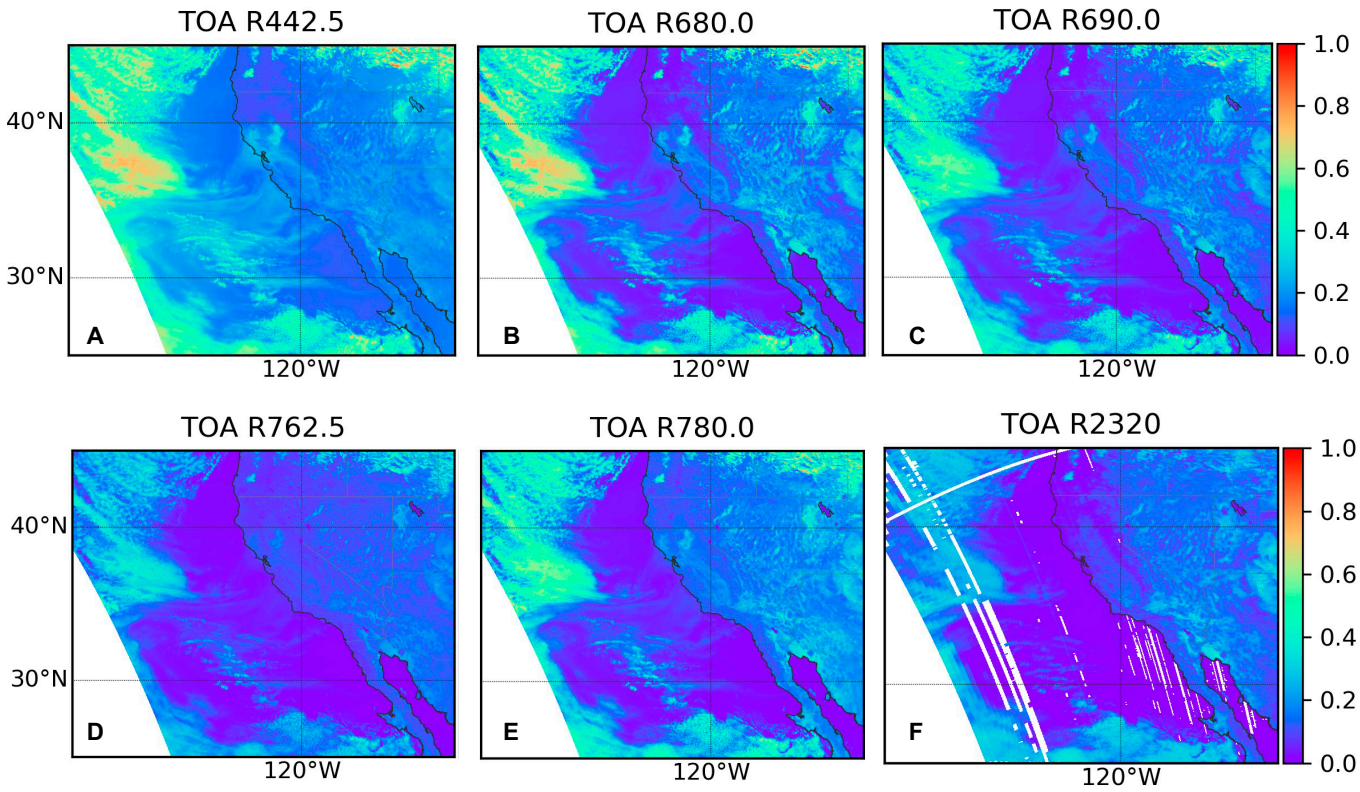

Fig. 4. TROPOMI observed top-of-the-atmosphere (TOA) reflectance over the western United States on 2018 November 10 19:50 UTC spectrally convolved to 5 selected OCI bands of 442.5 nm (A), 680 nm (B), 690 nm (C), 672.5 nm (D), and 780 nm (E). Also shown is the TROPOMI observed reflectance in the 2,320-nm band (F), a proxy to OCI's 2,130-nm bands.

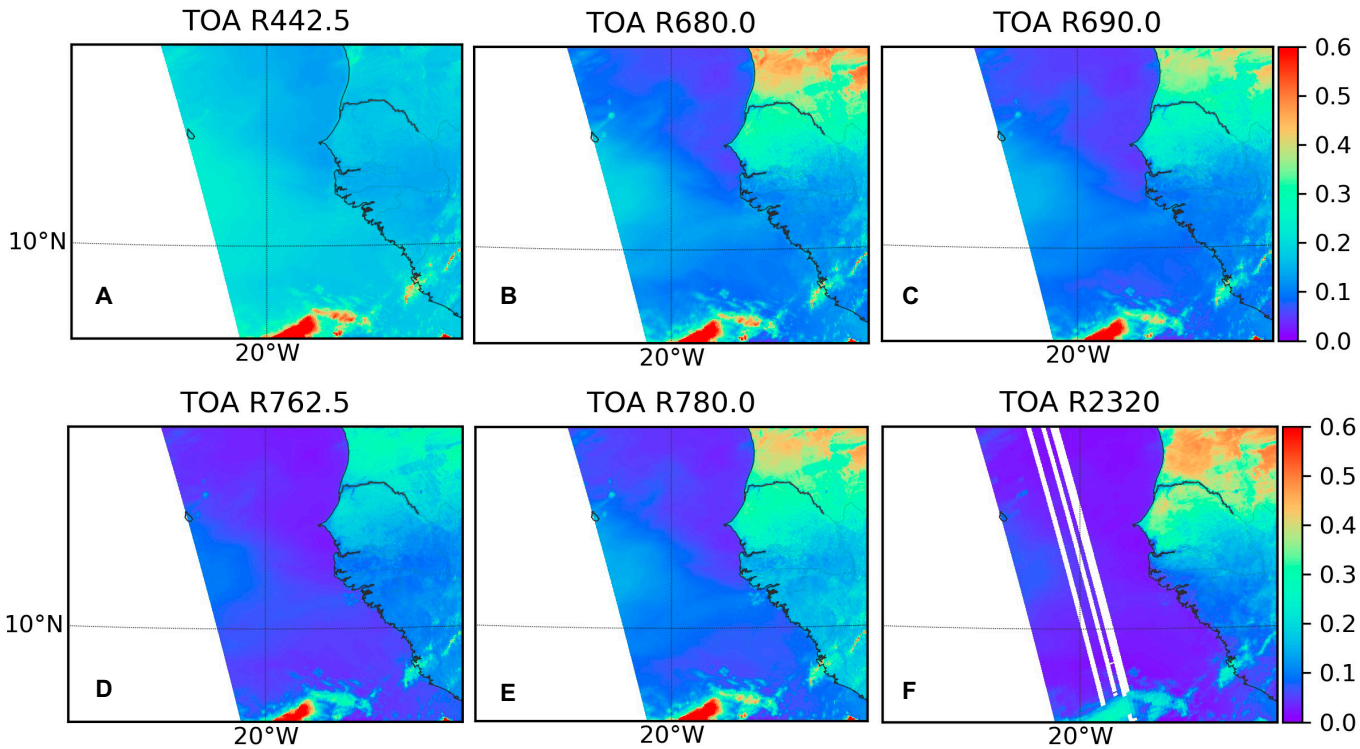

Fig. 5. Same as Fig. 4 but for TROPOMI observed reflectance spectrally convolved to OCI bands over the western coast of Africa on 2019 March 2 13:07 UTC. These panels show reflectance in the OCI bands of 442.5 nm (A), 680 nm (B), 690 nm (C), 672.5 nm (D), 780 nm (E), and 2,320 nm (F).

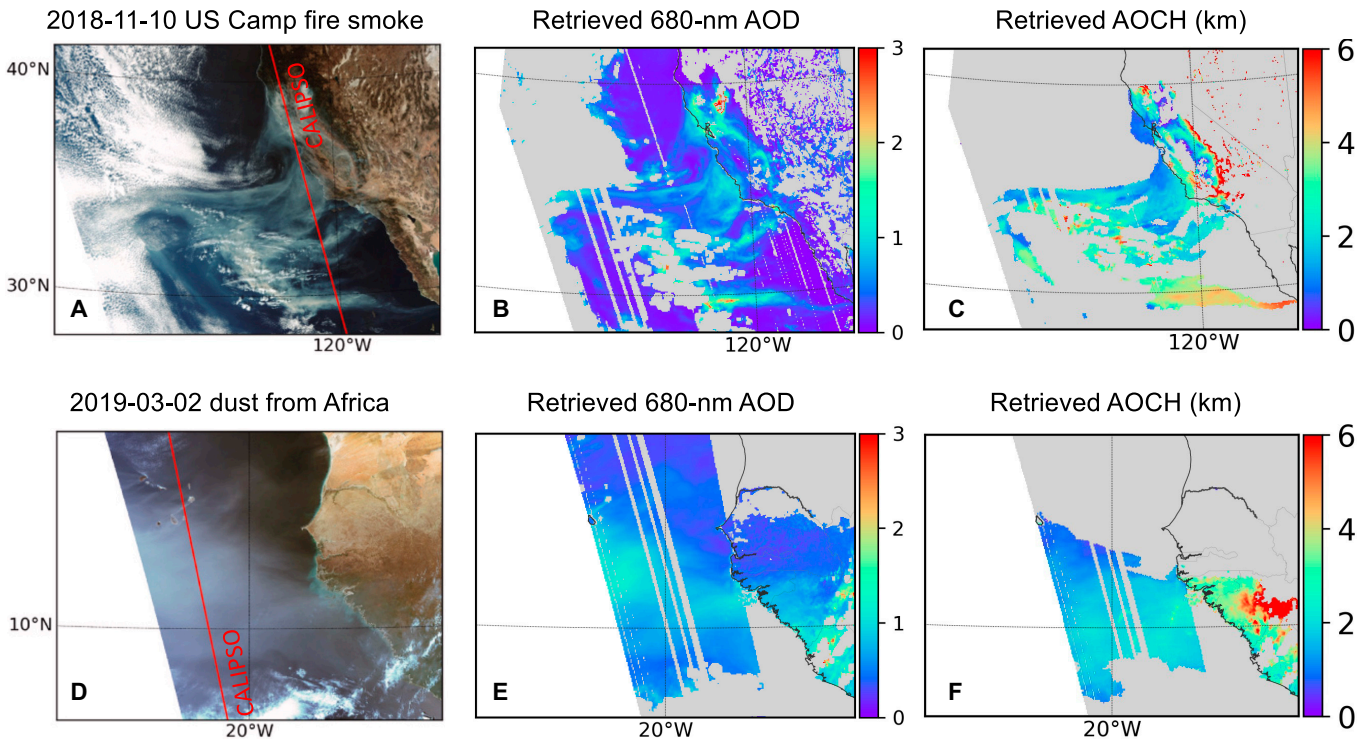

Fig. 6. Retrieved AOD (B and E) and AOCH (C and F) from the above OCI proxy observations. (A) and (D) display true-color TROPOMI images showing biomass smoke plumes, and the red line indicates ground track of the CALIPSO satellite passing through within about 1.5 h.

and AOCH retrievals from marine to land surfaces. However, high AOCH values associated with the smoke cases over land should be approached with caution as they are potentially impacted by cloud contamination. The high AOCH values for the dust event over land are likely caused by smoke contaminations that were emitted from the vegetated surface over West Africa areas.

CALIOP-detected aerosol extinction profiles (Fig. 7), whose orbit tracks are shown in the RGB images in Fig. 6, were used to evaluate the retrieved AOCH results from proxy OCI data. The quantitative assessment involved the calculation of an extinction-weighted height derived from cloud-screened CALIOP aerosol extinction profiles, which are indicated by the black curves in Fig. 7A and C. The AOCH retrievals from the proxy OCI data were then collocated with CALIOP observations, presented as brown curves, which revealed a consistent pattern along the CALIOP orbital track. Here, we use the CALIOP 532-nm particulate extinction profile for smoke ALH evaluation and the 1,064-nm extinction profile for dust ALH evaluation, considering the different spectral variability of smoke and dust extinction relative to molecular scattering.

The quantitative analysis, depicted in Fig. 7B and D through scatter plots between OCI retrievals and CALIOP lidar measurements, yielded a strong agreement and high correlation coefficient. The precision of these retrievals, marked by an uncertainty (i.e., the root mean square error [RMSE] between CALIOP data and AOCH retrievals) of less than 0.5 km, is consistent with the findings from previous studies utilizing DSCOVR/EPIC and TROPOMI observations (e.g., [8,10]), suggesting OCI's potential for providing a robust aerosol height product and will contribute to our understanding of aerosol distribution and impacts.

Conclusion

This study evaluates the capability of the OCI on NASA's PACE satellite to determine the height of aerosol layers over the ocean surface by using the oxygen A and B absorption bands. Through radiative transfer simulations and utilizing proxy OCI data derived from the TROPOMI observations for both smoke and dust aerosol events, we have identified most informative OCI bands and demonstrated their potential in aerosol height retrievals. The key findings from this study can be summarized as follows:

- OCI observations around the oxygen A bands are found to be strongly sensitive to the ALH over oceanic surfaces, whereas those in the oxygen B bands demonstrate relatively reduced sensitivity.
- The most pronounced sensitivity to ALH is found in the 762.5 nm (and 690 nm) around the oxygen A (and B) bands, which are selected for ALH retrievals in this study.
- The ALH retrieved from OCI proxy data, which has been spectrally convolved from TROPOMI observations, aligns closely with the aerosol profile probed by the CALIOP lidar. The AOCH retrievals for both smoke and dust aerosol events present an RMSE of 0.49 km and 0.31 km, respectively, for the smoke and dust events, which is similar to the uncertainties of AOCH as retrieved from the DSCOVR EPIC and TROPOMI instruments.

The outcomes regarding sensitivity and retrieval exercises from this study suggest that a promising and robust ALH product could be produced from PACE's OCI observations over oceans. It is important to note, however, that the current

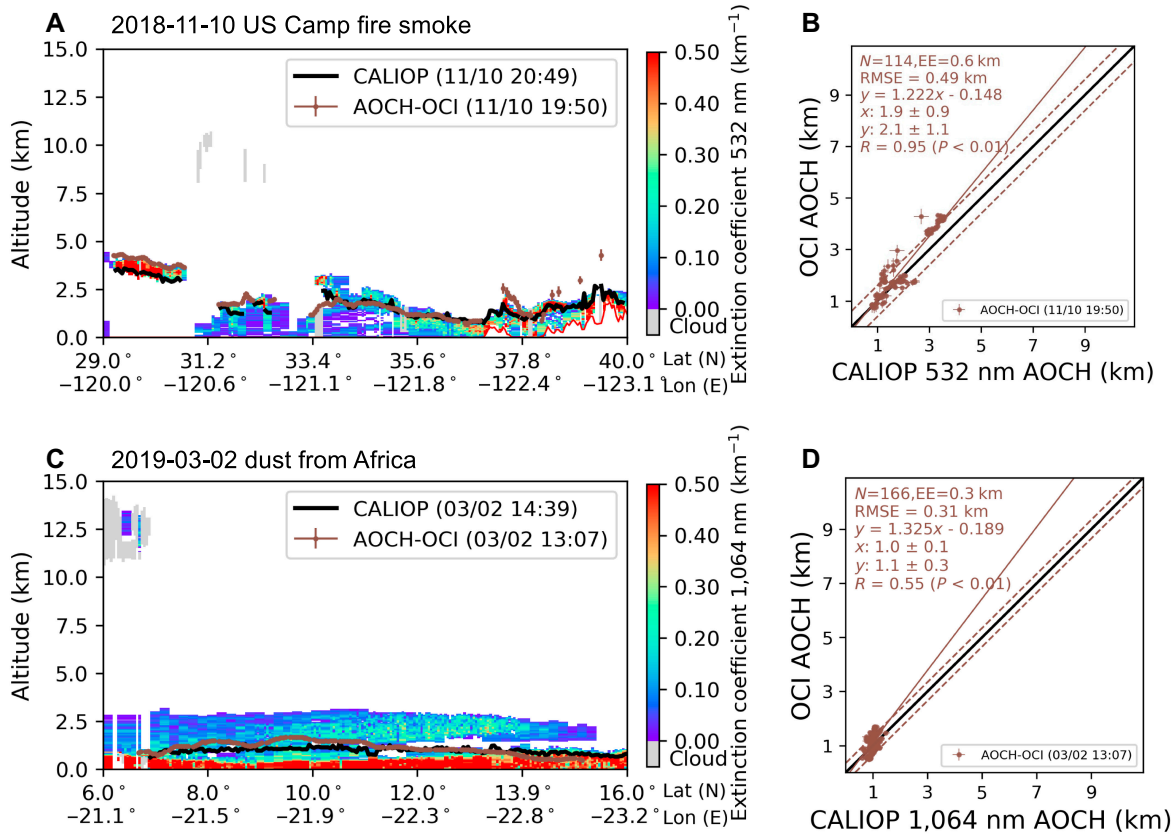

Fig. 7. A comparison of OCI-retrieved ALH with aerosol extinction profile probed by CALIOP lidar for both the smoke (A and B) and dust (C and D) events. (A and C) CALIOP retrieved aerosol extinction profile and OCI AOCH retrievals (brown curves) along the CALIOP orbital track. Blue curves indicate an extinction weighted AOCH from CALOP profile. (B and D) Scatter plots of OCI AOCH versus CALIOP AOCH annotated with comparison statistics.

study's findings were predicated upon TROPOMI-derived proxy measurements. While this study demonstrated the capability of OCI observations in the oxygen absorption bands for retrieving ALH, the data used in this study are derived from TROPOMI measurements. The retrieval errors within actual OCI deployment may vary, depending on actual observation uncertainty and algorithm implementations. Nevertheless, a notable deviation is not anticipated, given the retrieval principles remaining the same and the consistent application of observation data from other instruments.

The methodology of this study, designed to showcase the OCI's retrieval capability, intentionally simplified or omitted some steps in the practical retrieval development. Those include cloud screening and the utilization of the aerosol index for detecting the presence of absorbing aerosol layers. The cloud screening in this study was inherited from Chen et al. [8] without further refinement for OCI data. The aerosol index step was omitted given that the selected case events are for absorbing smoke and dust. However, it should be noted that OCI observations include bands for aerosol index calculation, and this step must be incorporated when the presented algorithm is applied to OCI real data.

While this study focuses on ALH over ocean surfaces, the retrieval results included AOCH retrieval over land surfaces. Although necessitating further assessment, our AOCH retrievals show a smooth transition from ocean to land surfaces, indicating the potential capability of OCI data for AOCH retrieval over land. In addition, it is worthwhile to synergize the aerosol height information from this study with other technical aspects of PACE observations. This includes comparing with parallax height retrievals and leveraging multi-angle polarimetric data within the blue bands to refine and enhance the accuracy of aerosol height measurements.

Acknowledgments

We thank the support of this study from the PACE Science Project Team and valuable interaction with the PACE Science and Application Science Team. We also acknowledge the computing support from UMBC High Performance Computing Facility and U Iowa High Performance Computing resources.
Funding: The authors declare that financial support was received for the research, authorship, and/or publication of this article. This research was funded by the NASA Remote Sensing Theory program (Grant No. 80NSSC20K1747), the DSCOVR program (Grant No. 80NSSC22K0503), and the UMBC START and CIDER awards.
Author contributions: X.X.: Conceptualization, funding acquisition, investigation, methodology, validation, visualization, and writing—original draft. X.C.: conceptualization, data curation, methodology, visualization, and writing—review and editing. J.W.: Conceptualization, funding acquisition, investigation, methodology, and writing—review and editing. L.R.: Data curation, methodology, and writing—review and editing.
Competing interests: The authors declare that they have no competing interests.

Data Availability

The original contributions presented in the study are included in the article material; further inquiries can be directed to the corresponding authors.

References

1. Remer LA, Davis AB, Mattoo S, Levy RC, Kalashnikova OV, Coddington O, Chowdhary J, Knobelspiesse K, Xu X, Ahmad Z, et al. Retrieving aerosol characteristics from the PACE Mission, part 1: Ocean color instrument. *Front Earth Sci*. 2019;7:152.
2. Werdell PJ, Behrenfeld MJ, Bontempi PS, Boss E, Cairns B, Davis GT, Franz BA, Gliese UB, Gorman ET, Hasekamp O, et al. The plankton, aerosol, cloud, ocean ecosystem mission status, science, advances. *Bull Am Meteorol Soc*. 2019;100:1775–1794.
3. Gordon HR. Evolution of ocean color atmospheric correction: 1970–2005. *Remote Sens*. 2021;13(24):5051.
4. Duforêt L, Frouin R, Dubuisson P. Importance and estimation of aerosol vertical structure in satellite ocean-color remote sensing. *Appl Opt*. 2007;46(7):1107–1119.
5. Gordon HR, Du T, Zhang T. Remote sensing of ocean color and aerosol properties: Resolving the issue of aerosol absorption. *Appl Opt*. 1997;36(33):8670–8684.
6. Xu X, Wang J, Wang Y, Kokhanovsky A. Passive remote sensing of aerosol height. In: Islam T, Hu Y, Kokhanovsky A, Wang J, editors. *Remote Sensing of Aerosols, Clouds, and Precipitation*. Cambridge (MA): Elsevier; 2018. p. 1–22.
7. Lin Y, Takano Y, Gu Y, Wang Y, Zhou S, Zhang T, Zhu K, Wang J, Zhao B, Chen G, et al. Characterization of the aerosol vertical distributions and their impacts on warm clouds based on multi-year ARM observations. *Sci Total Environ*. 2023;904:166582.
8. Chen X, Wang J, Xu X, Zhou M, Zhang H, Castro Garcia L, Colarco PR, Janz SJ, Yorks J, McGill M, et al. First retrieval of absorbing aerosol height over dark target using TROPOMI oxygen B band: Algorithm development and application for surface particulate matter estimates. *Remote Sens Environ*. 2021;265:112674.
9. Lu Z, Wang J, Xu X, Chen X, Kondragunta S, Torres O, Wilcox EM, Zeng J. Hourly mapping of the layer height of thick smoke plumes over the Western U.S. in 2020 severe fire season. *Front Remote Sens*. 2021;2:766628.
10. Xu X, Wang J, Wang Y, Zeng J, Torres O, Reid JS, Miller SD, Martins JV, Remer LA. Detecting layer height of smoke aerosols over vegetated land and water surfaces via oxygen absorption bands: Hourly results from EPIC/DSCOVR in deep space. *Atmos Meas Tech*. 2019;12(6):3269–3269.
11. Kalashnikova OV, Garay MJ, Davis AB, Diner DJ, Martonchik JV. Sensitivity of multi-angle photo-polarimetry to vertical layering and mixing of absorbing aerosols: Quantifying measurement uncertainties. *J Quant Spectrosc Radiat Transf*. 2011;112(13):2149–2163.
12. Wu L, Hasekamp O, van Diedenhoven B, Cairns B, Yorks JE, Chowdhary J. Passive remote sensing of aerosol layer height using near-UV multiangle polarization measurements. *Geophys Res Lett*. 2016;43(16):8783–8790.
13. Moroney C, Davies R, Muller J-P. Operational retrieval of cloud-top heights using MISR data. *IEEE Trans Geosci Remote Sens*. 2002;40(7):1532–1540.
14. Muller J-P, Mandanayake A, Moroney C, Davies R, Diner DJ, Paradise S. MISR stereoscopic image matchers: Techniques and results. *IEEE Trans Geosci Remote Sens*. 2002;40(7):1547–1559.
15. Meister G, Knuble JJ, Gliese U, Bousquet R, Chemerys LH, Choi H, Eplee RE, Estep RH, Gorman ET, Kitchen-McKinley S, et al. The ocean color instrument (OCI) on the Plankton, Aerosol, Cloud, ocean Ecosystem (PACE) mission: System design and prelaunch radiometric performance. *IEEE Trans Geosci Remote Sens*. 2024;62:5517418.
16. Veefkind JP, Aben I, McMullan K, Förster H, de Vries J, Otter G, Claas J, Eskes HJ, de Haan JF, Kleipool Q, et al. TROPOMI on the ESA Sentinel-5 precursor: A GMES mission for global observations of the atmospheric composition for climate, air quality and ozone layer applications. *Remote Sens Environ*. 2012;120:70–83.
17. Ding S, Wang J, Xu X. Polarimetric remote sensing in oxygen A and B bands: Sensitivity study and information content analysis for vertical profile of aerosols. *Atmos Meas Tech*. 2016;9:2077–2092.
18. Dubuisson P, Frouin R, Dessailly D, Duforêt L, Léon JF, Voss K, Antoine D. Estimating the altitude of aerosol plumes over the ocean from reflectance ratio measurements in the O_2 A-band. *Remote Sens Environ*. 2009;113(9):1899–1911.
19. Xu X, Wang J, Wang Y, Zeng J, Torres O, Yang Y, Marshak A, Reid J, Miller S. Passive remote sensing of altitude and optical depth of dust plumes using the oxygen A and B bands: First results from EPIC/DSCOVR at Lagrange-1 point. *Geophys Res Lett*. 2017;44(14):7544–7554.
20. Wang J, Xu X, Ding S, Zeng J, Spurr R, Liu X, Chance K, Mishchenko M. A numerical testbed for remote sensing of aerosols, and its demonstration for evaluating retrieval synergy from a geostationary satellite constellation of GEO-CAPE and GOES-R. *J Quant Spectrosc Radiat Transf*. 2014;146:510–528.
21. Xu X, Wang J. UNL-VRTM, a testbed for aerosol remote sensing: Model developments and applications. In: Kokhanovsky A, editor. *Springer Series in Light Scattering*. Springer: 2019. p. 1–69.
22. Spurr R, Christi M. The LIDORT and VLIDORT linearized scalar and vector discrete ordinate radiative transfer models: Updates in the last 10 years. In: Kokhanovsky A, editor. *Springer Series in Light Scattering*. Springer; 2019. p. 1–62.
23. Spurr RJD. VLIDORT: A linearized pseudo-spherical vector discrete ordinate radiative transfer code for forward model and retrieval studies in multilayer multiple scattering media. *J Quant Spectrosc Radiat Transf*. 2006;102(2):316–342.
24. Hou W, Wang J, Xu X, Reid JS, Han D. An algorithm for hyperspectral remote sensing of aerosols: 1. Development of theoretical framework. *J Quant Spectrosc Radiat Transf*. 2016;178:400–415.
25. Xu X, Wang J, Zeng J, Hou W, Meyer KG, Platnick SE, Wilcox EM. A pilot study of shortwave spectral fingerprints of smoke aerosols above liquid clouds. *J Quant Spectrosc Radiat Transf*. 2018;221:38–50.
26. Li C, Xu X, Liu X, Wang J, Sun K, van Geffen J, Zhu Q, Ma J, Jin J, Qin K, et al. Direct retrieval of NO_2 vertical columns from UV-vis (390-495 nm) spectral radiances using a neural network. *J. Remote Sens*. 2022;2022:9817134.
27. Pearlman A, Cook M, Efremova B, Padula F, Lamsal L, McCorkel J, Joiner J. Polarization performance simulation

for the GeoXO atmospheric composition instrument: NO_2 retrieval impacts. *Atmos Meas Tech*. 2022;15(15):4489–4501.

28. Kaufman YJ, Tanré D, Boucher O. A satellite view of aerosols in the climate system. *Nature*. 2002;419(6903):215–223.